Journal of Materials Chemistry C

ROYAL SOCIETY OF CHEMISTRY

PAPER

View Article Online
View Journal | View Issue

Cite this: J. Mater. Chem. C, 2025, 13, 12890

Old dog, new trick: discovery of the solid-state phthalate detection capabilities of fluorescein†

Pablo Labra-Vázquez,*[a] Marie Gressier,[a] Guillaume Rioland [b] and Marie-Joëlle Menu *[a]

Received 12th March 2025,
Accepted 12th May 2025

DOI: 10.1039/d5tc01078k

rsc.li/materials-c

This manuscript presents the development of fluorescent materials capable of detecting di-(2-ethylhexyl)phthalate (**DEHP**) vapors, which is an important concern for the airspace industry, as during the preparation and on-orbit life of satellites and other spacecraft, phthalate vapors deposit on sensitive optical systems, hampering their proper functioning. Here we present a novel approach for the detection of this contaminant, with a rational design of the materials supported by DFT computations. Our main approach involved the solid-state optical detection of **DEHP** *via* photoinduced electron transfer, as a novel phthalate detection strategy. While the pursued response was gratifyingly observed for most of the investigated fluorophores, the detection capabilities of materials containing fluorescein were discovered to be unique, significantly outperforming the other fluorophores. Furthermore, an unanticipated solid-state ratiometric response towards **DEHP** was observed for fluorescein, displaying a particularly high contrast that allowed a naked-eye detection of the contaminant. The molecular mechanism behind the unique response of fluorescein was investigated in detail both experimentally and theoretically, allowing us to propose a detection mechanism for fluorescein through a **DEHP**-induced tautomerization between the zwitterionic and the lactoid tautomer of the fluorophore.

Introduction

Phthalates are a class of plasticizers used in the production of polyvinyl chloride (PVC) based plastics that make up a great variety of daily-use goods, from bags and construction materials to food packages and drinking-water bottles.[1] Inclusion of phthalates brings significant improvements to plastics, helping overcome the rigidity and thermal instability of pure PVC.[2] Unfortunately, due to their noncovalent attachment, these plasticizers are slowly released into the environment. Because of the toxicity that has been demonstrated for various phthalates, including carcinogenic, teratogenic and endocrine-disrupting properties,[3] these chemicals have been at the focus of diverse regulatory agencies across the globe, leading to one of the most used phthalates, di-(2-ethylhexyl)phthalate (**DEHP**) being formally classified as a CMR1B (Carcinogenic Mutagenic or Reprotoxic) substance.[4] In spite of these efforts, alarming contamination levels continue to be found in drinking water and food-contact materials.[5] This has raised significant interest in the development of sensors and analytical assays for the detection and quantification of these contaminants, which compared to instrumental methods such as HPLC/GC/MS, can be less expensive and easier to transport and operate, among other practical advantages, depending on the physicochemical property transduced by the sensor.[6]

Due to the need of minimizing human exposure to phthalates, most sensors target phthalate detection and quantification in aqueous samples. Nonetheless, vapors of these contaminants also pose serious problems which are significantly less acknowledged. Indeed, phthalate vapors constitute important contaminants for the airspace industry, affecting the proper functioning of spacecraft and diverse on-board devices as they deposit on the surface of critical components. In this context, contamination by phthalates can occur during all the life of spacecraft, from the diverse ground preparation stages where they are subjected to repeated vacuum cycles, to on-orbit flight where these devices are exposed to the extreme hostile conditions of outer space. The situation is particularly problematic for optical components such as solar cells[7] and charge-coupled device (CCD) cameras,[8] which are critical for research and for orientation and navigation. It is therefore of utmost importance to assess surface contamination of spacecraft to ensure that these critical optical components remain operative during long periods of time. Before launch, the

[a] CIRIMAT, Université de Toulouse, CNRS, Université Toulouse 3 – Paul Sabatier, 118 Route de Narbonne, 31062, Toulouse, Cedex 9, France.
E-mail: pab.labra@gmail.com, marie-joelle.menu@univ-tlse3.fr
[b] Centre National d'Etudes Spatiales, DTN/QE/LE, 31401, Toulouse, France

† Electronic supplementary information (ESI) available: Copies of NMR and optical absorption and fluorescence spectra, experimental details and procedures and computational methods. CCDC 2407098 and 2407099. For ESI and crystallographic data in CIF or other electronic format see DOI: https://doi.org/10.1039/d5tc01078k

most common approach for the assessment of surface contamination is the use of Quartz Crystal Microbalance (QCM) devices, which although highly precise, involve sequential unitary operations which can become impractical and time-consuming.

In this context, the development of optical sensors for contamination by phthalate vapors can potentially help overcome these limitations by enabling a continuous and real-time assessment of the surface contamination in spacecraft. Unfortunately, optical sensors for the detection of phthalate vapors remain largely unexplored, which may in part be due to their poor optical properties, with both an absorption restrained to the UV region and a negligible fluorescence, making it difficult to develop sensitive optical sensors. Only recently a study has delved into the subject, using a detection system based on the fluorescence enhancement induced by phthalates due to the restriction of motion on a nanostructured fluorenyl derivative.[9] Even though the fluorescence enhancement was modest, with the system exhibiting a single emissive band, the analytical response of the material allowed a very sensitive detection of phthalates even from complex samples.

In this contribution we report on the results of a research program directed towards evaluating photoinduced electron transfer (PET) as an alternative detection mechanism for phthalate vapors. The screening, selection and testing of various fluorophores revealed an outstanding fluorescent response for fluorescein, which displayed an unexpected solid-state dual emission that allowed a ratiometric detection of **DEHP**, which was used as a representative phthalate throughout the study. Fluorescent materials built from fluorescein allowed not only a sensitive detection of the contaminant, but also a naked-eye detection thanks to a remarkable visual contrast provided by its ratiometric response. The manuscript is organized as follows: first, we will present the screening and validation of the various fluorophores involved in the PET detection strategy, including both experimental and computational investigations that demonstrate the viability of these fluorophores for participating in PET with **DEHP**. This is followed by a discussion on their solid-state performance towards the detection of **DEHP** from organic solutions and vapors, with a focus on the remarkable response observed for fluorescein. The manuscript finishes by presenting a potential mechanism explaining the interesting ratiometric response of fluorescein, which is proposed to occur due to a **DEHP**-induced tautomerization of the fluorophore.

Results and discussion

Experimental design and validation of the detection method

As a first approach towards the detection of phthalate vapors, PET was targeted as a potential detection mechanism. This approach was selected to overcome the difficulties caused by the poor optical properties of phthalates, which preclude their direct visual detection. An alternative approach based on PET would exploit the optical properties of fluorophores with strong optical absorption and emission, as well as their capacity to transfer an electron to the phthalate upon photoexcitation. This process would compete with the emission of the fluorophores, leading to a quenching of their emission in the presence of phthalate vapors, thus offering an indirect visual detection of these contaminants.

The investigation commenced with an examination of fluorophores that exhibited the requisite electronic properties for the detection of phthalates by PET. As previously stated, **DEHP** was selected as a model phthalate throughout this study due to its high relevance as a contaminant in spacecraft. As illustrated in Fig. 1(a), the proposed PET detection process involves **DEHP** acting as the electron acceptor, while the different fluorophores are employed as donors. The search for suitable fluorophores was initially conducted computationally, with a large group of molecules screened using DFT computations at the M06-2X/6-31+G(d,p) level of theory. Our investigation was centered on the relative energy of the frontier molecular orbitals (FMOs) of the fluorophores ($E^{\mathrm{DFT}}_{\mathrm{HOMO/LUMO}}$) with respect to those of **DEHP**. The most crucial selection criterion was the presence of a lowest unoccupied molecular orbital (LUMO) in the fluorophore above that in **DEHP**, allowing for an electron transfer (ET) to occur between these orbitals.

Following an inspection of the $E^{\mathrm{DFT}}_{\mathrm{HOMO/LUMO}}$ energies, along with some practical considerations (*e.g.*, commercial availability), five fluorophores were selected from a large library of candidates. The selected fluorophores were 9*H*-fluorene (**F**), 9,9-dioctylfluorene (**FO**), 9-methylcarbazol (**C**), pyrene (**P**), and fluorescein in its lactoid tautomer (**FL**). It is important to clarify the rationale behind the selection of **FL**, as this tautomer of fluorescein and closely related derivatives are frequently referred to as nonfluorescent.[10] This choice may thus appear counterintuitive. However, as will be discussed in detail subsequently, our present study challenges this notion by presenting a comprehensive characterization of the optical properties of **FL**, which we have found to exhibit blue fluorescence.

The computational screening described above was also employed to investigate the fluorophores selected for their potential relevance to PET. This involved corroborating the energy of their FMOs, which was identified as being of paramount importance for PET. It should be noted that both the experimental and computational inspection of the energy of the FMOs were carried out in acetonitrile, which is a common solvent in PET studies due to its high polarity, which helps to stabilize significantly polarized species, such as those produced during PET.[11] The experimental investigation was conducted by determining the redox potentials of these molecules using cyclic voltammetry (CV) measurements.[12] The results are presented in Fig. 1(b) and Table 1. It is noteworthy that the DFT method employed consistently overestimated the energy band-gap (E_g^{DFT}) when compared to the electrochemical values (E_g^{CV}). Notwithstanding the typical constraints associated with DFT,[13] the overall concordance between the experimental and computational trends is nonetheless satisfactory. It is of particular significance that the energy of the LUMO level of the fluorophores was indeed satisfactorily found to be higher than that of **DEHP**. Notwithstanding the apparent exception for **P**, whose LUMO level is predicted by DFT to be located 0.33 eV

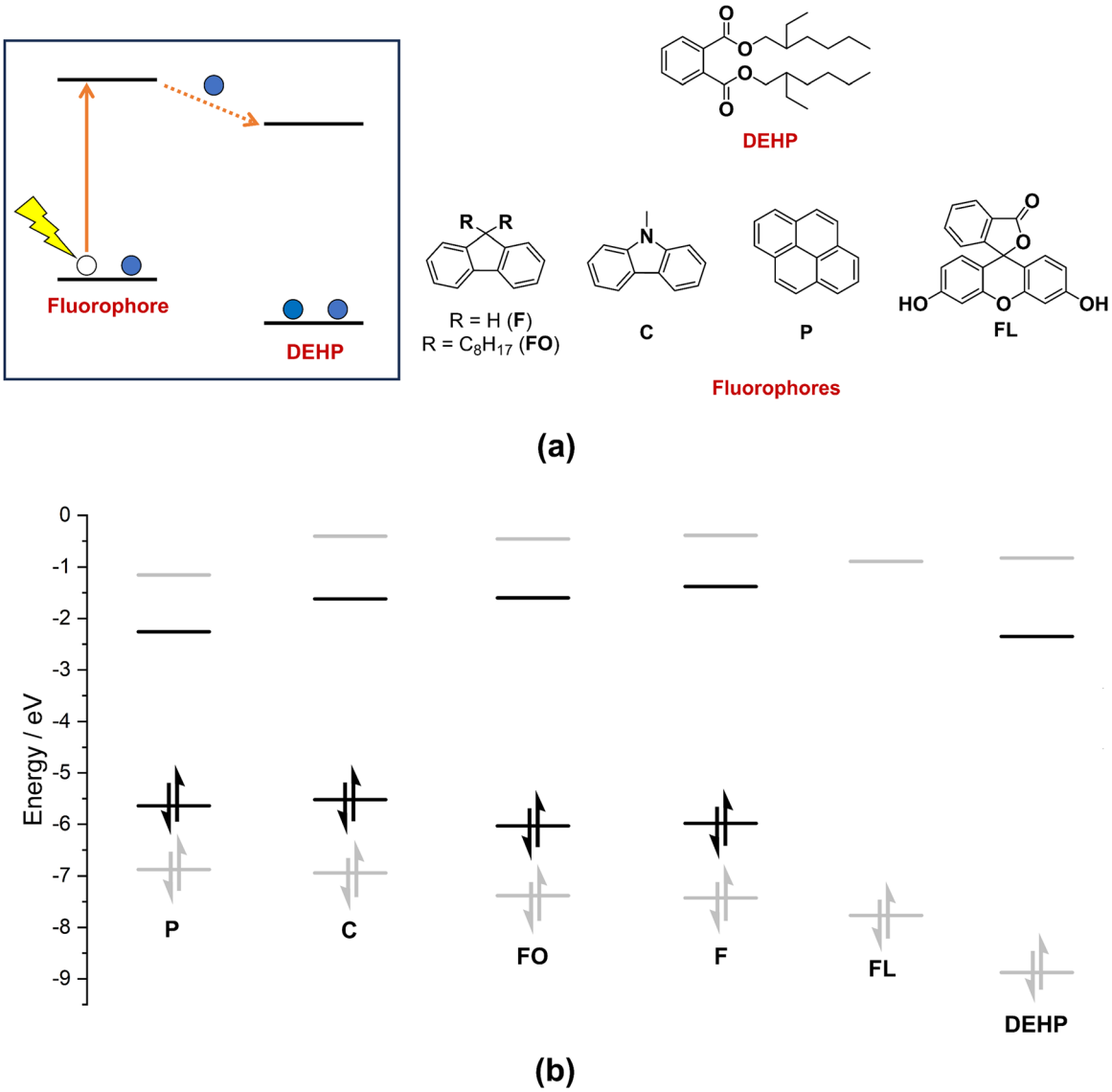

Fig. 1 (a) Schematic representation of the proposed photoinduced electron transfer (PET) process between the target contaminant (**DEHP**) and the different fluorophores (b) Frontier molecular orbital (FMO) energy diagram derived from cyclic voltammetry (black lines) and DFT computations (M06-2X/6-31+G**/PCM, gray lines) in acetonitrile. Some FMO energies (for **FL** and **DEHP**) could not be estimated electrochemically.

below that of **DEHP**, experimental findings indicate that it lies energetically above by approximately 0.09 eV. A comparable scenario is also predicted by DFT for **FL**, however, with a considerably lower energy difference between the LUMO of **FL** and **DEHP** (0.07 eV). Although electrochemical data for **FL** could not be recorded in acetonitrile to eliminate this uncertainty due to chemical instability (see ESI,† Section S2), the difference was deemed not significant.

Table 1 Oxidation and reduction potentials ($E^{(i)}_{ox/red}$, *vs.* SCE), frontier orbital energies ($E^{CV}_{HOMO/LUMO}$) and energy bandgap (E^{CV}_{g}) in acetonitrile determined from CV measurements. Values computed by DFT at the M06-2X/6-31+G(d,p)/PCM level of theory ($E^{DFT}_{HOMO/LUMO}$, E^{DFT}_{g}) are presented in parentheses

	$E^{(i)}_{ox}$/V	$E^{(i)}_{red}$/V	$E^{CV}_{HOMO}(E^{DFT}_{HOMO})$/eV	$E^{CV}_{LUMO}(E^{DFT}_{LUMO})$/eV	E^{CV}_{g} (E^{DFT}_{g})/eV
DEHP	—[a]	−2.045	—[a] (−8.88)	−2.35 (−0.82)	—[a] (8.06)
FL	—[b]	—[b]	—[b] (−7.77)	—[b] (−0.89)	—[b] (6.88)
F	1.58	−3.02	−5.98 (−7.43)	−1.38 (−0.39)	4.60 (7.04)
FO	1.63	−2.80	−6.03 (−7.38)	−1.60 (−0.46)	4.43 (6.92)
C	1.12	−2.78	−5.52 (−6.94)	−1.62 (−0.41)	3.90 (6.53)
P	1.24	−2.14	−5.64 (−6.87)	−2.26 (−1.15)	3.38 (5.72)

[a] Outside of the voltage window of acetonitrile. [b] Not determined due to chemical instability.

To further validate the PET detection approach, an investigation was conducted on the viability of forming favorable supramolecular interactions between **DEHP** and the fluorophores. This was done with consideration of the fact that ET rates are strongly dependent on intermolecular distances and orbital overlap.[14] Due to significant problems found on growing co-crystals of the analyte and the fluorophores, the investigation of these molecular adducts was undertaken using DFT. The results, detailed in ESI,† Section S3, evidence the possibility of forming stable aggregates between **DEHP** and all the fluorophores, exhibiting π-stacking interactions with relatively short intermolecular distances, held together by moderate to strong interaction energies. Furthermore, the change in Gibbs energy associated with the PET process (ΔG°_{PET}) was conveniently estimated obtained using the Rehm–Weller equation (eqn (1)):[15]

$$\Delta G^{\circ}_{PET} = F\left\{E^{i}_{ox}(D) - E^{i}_{red}(A)\right\} - E_{0,0} + C \qquad (1)$$

where F is Faraday's constant, $E^{i}_{ox}(D)$ is the oxidation potential of the electron donor (the fluorophore), $E^{i}_{red}(A)$ is the reduction potential of the acceptor (**DEHP**), $E_{0,0}$ is the zero-vibrational excitation energy of the fluorophore and **C** is a coulombic interaction term (*ca.* 0.03 eV in acetonitrile).[16] This robust methodology was successfully applied to fluorophores **F**, **FO**, **C**, and **P**, for which the redox potentials could be recorded. The ΔG°_{PET} values are shown in Table 2, along with optical data required to determine the $E_{0,0}$ (optical absorption and emission spectra can be consulted in ESI,† Section S4). As can be observed, the obtained ΔG°_{PET} values clearly indicate that PET between **DEHP** and these fluorophores is thermodynamically favored and should occur upon photoexcitation. It is important to clarify, however, that the optical properties of **DEHP** and the fluorophores also indicate the possibility of an inner filter effect occurring alongside PET. Indeed, the optical absorption of **DEHP** extends up to *ca.* λ = 290 nm, overlapping with the optical absorption of the fluorophores (see ESI,† Fig. S22), thus suggesting potential difficulties in discriminating the origins of the intended fluorescence quenching. Exceptions to this are **C** and **P**, whose optical absorption extends up to λ = 340–360 nm and could potentially be excited outside the optical window of **DEHP**.

In this section, we have presented our strategy for the detection of phthalate vapors, which was based on the use of PET as a sensing mechanism. A computational screening helped us identify five potential fluorophores, well-suited for participating as electron donors in PET with **DEHP** as a model acceptor. The investigation employed a combination of computational and experimental techniques, with a primary focus on the energy of the frontier molecular orbitals of the fluorophores in relation to **DEHP**. Additionally, the formation of stable supramolecular aggregates with significant orbital overlap with this phthalate was also unveiled by DFT. Ultimately, the Rehm–Weller equation was employed to ascertain the PET Gibbs free energy for most of the selected fluorophores, thereby demonstrating that the process is thermodynamically favored. While no further experiments were conducted to confirm the occurrence of PET, the presented evidence suggests that this phenomenon can be operative under photoexcitation of these fluorophores in the presence of **DEHP**. The following sections will present the fluorescence response towards **DEHP** as well as a detailed discussion on **FL**, which exhibited an exceptional response due to its distinctive structure, allowing it to switch between different tautomers with different optical properties in the presence of the phthalate.

Fluorescent response towards phthalate vapors

Having delineated our strategy for the detection of phthalate vapors, we will now present the optical response of the selected fluorophores to **DEHP**. We will initially present the response of fluorophores **F**, **FO**, **C** and **P**, for which similar responses were recorded when exposed to the contaminant. We will then present our findings on **FL**, which exhibited a distinctive response associated with the possibility for this molecule to tautomerize among different forms. The employed methodology was based on the utilization of **DEHP**-indicating test papers, following recent reports on the efficacy of this technique for the detection of TNT.[11c,17] To this end, test papers were prepared by absorbing diluted solutions of each fluorophore in filter papers, followed by their subsequent exposure to either solutions or vapors of **DEHP**. The fluorescence spectra were subsequently recorded to evaluate the extent of fluorescence quenching in the presence of **DEHP**, as anticipated by our PET detection approach.

Prior to examining the response of the fluorophores to **DEHP** vapors, calibration curves for each fluorophore were constructed using **DEHP** solutions with the objective of subsequently extrapolating quantitative data regarding the quantity of **DEHP** vapors deposited on the test papers. The calibration curves allow correlating **DEHP** concentration with fluorescence

Table 2 Optical absorption and emission properties, zero-vibrational electronic excitation energy (E_{00}) and PET Rehm–Weller Gibbs energies (ΔG°_{PET}) in acetonitrile

	λ^{abs}_{max}/nm (ε/M^{-1} cm^{-1})	λ^{em}_{max}/nm	$\Delta\lambda$/nm	$\Delta\nu$/cm^{-1}	E_{00}/eV	ΔG°_{PET}/kJ mol^{-1}
DEHP	223 (25 800)	—	—	—	—	—
FL[a]	275 (7300)	425	150	13 104	3.54	—[b]
F	262 (19 900)	315	53	6422	4.30	−62.23
FO	264 (16 600)	317	53	6333	4.27	−54.51
C	292 (15 000)	368	76	7072	3.76	−54.51
P	334 (44 400)	372	38	3058	3.48	−15.91

[a] Data recorded from a freshly prepared analytical sample of the compound as an acetone solvate (**FL-Me$_2$CO**). [b] Not determined due to chemical instability during CV measurements.

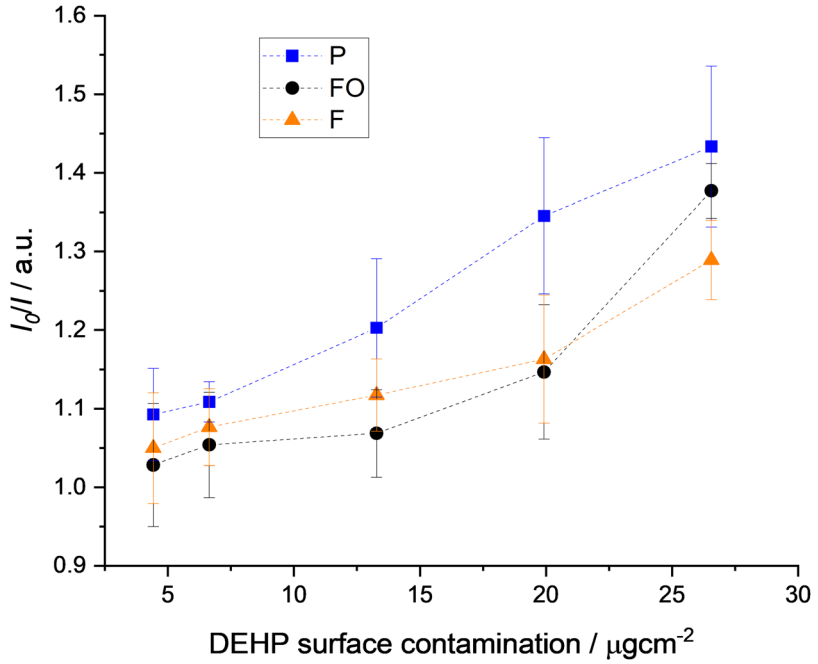

Fig. 2 Influence of the **DEHP** surface contamination on the fluorescence quenching in the solid state for fluorophores **F**, **FO** and **P** at λ_{exc} = 285 nm. The fluorescence quenching is given by the I_0/I ratio, where I_0 is the fluorescence intensity in the absence of **DEHP** and I is the fluorescence intensity in the presence of a given **DEHP** surface contamination value.

quenching, as indicated by the I_0/I ratio, where I_0 and I represent the fluorescence intensity in the absence or presence of a given concentration of **DEHP**, respectively. The calibration curves were obtained by depositing 5 μL drops of pentane solutions of **DEHP** at varying concentrations on a single test paper, followed by measuring the fluorescence spectra using a custom-built optical setup (ESI,† Fig. S23). It should be noted that, in the context of our research project, our objective was to estimate surface contamination values rather than **DEHP** concentrations. Accordingly, the discussion of surface contamination is presented in terms of micrograms per square centimeter, as opposed to molar concentrations. The surface contamination values were calculated assuming a perfectly circular dispersion of the drops within the papers. Although this constitutes a potentially significant approximation, we deemed it an appropriate exploratory approach to evaluate the efficacy of the fluorophores in signaling the degree of contamination by **DEHP** on a surface.

As previously stated, fluorophores **F**, **FO**, **C**, and **P** exhibited comparable behavior, with fluorescence becoming increasingly quenched as **DEHP** surface contamination values increased. However, an analytical issue was identified for **C**, which, despite displaying a favorable qualitative response, yielded unstable fluorescence spectra during the measurements. Consequently, the results for this fluorophore will not be discussed in this context. On the other hand, the responses observed for **F**, **FO** and **P** are shown in Fig. 2, where an increasing quenching of the fluorescence is observed in the 4.42 to 26.55 mg cm^{-2} interval, with uncertainties in the I_0/I value between 2.6 and 7.6%. The best response was observed for **P**, which showed the highest sensitivity and up to *ca.* 30% fluorescence quenching at the highest **DEHP** concentration. Test papers embedded with these fluorophores were also subjected to an atmosphere of **DEHP** vapors. Although clear differences in the fluorescence spectra were observed in the presence of **DEHP** vapors, the I_0/I values were too low (around I_0/I = 1.01 for **P** and 1.08 for **F** and **FO**) implying that although these materials might be useful for the detection of **DEHP** vapors, they could hardly be used to quantify them, especially considering the uncertainty observed in these measurements. Nonetheless, our interest at this point lied on screening the various fluorophores to eventually select the most sensitive, while the various experimental conditions that cause these analytical issues will be addressed in the future.

These experiments were also performed for fluorescein, whose optical response towards **DEHP** was gratifyingly found to outperform all the other fluorophores. The results are presented in Fig. 3, depicting the dual emission observed for this fluorophore with emission maxima around λ_{em} = 413 and 517 nm. The band centered around λ_{em} = 413 nm can be readily associated with the lactoid tautomer of fluorescein (**FL**) which as mentioned before displays a blue emission in acetonitrile (λ_{em} = 425 nm). The second band is responsible of a yellow emission centered a λ_{em} = 517 nm, and originates from a different fluorescein species, assigned to the zwitterionic tautomer (**FZ**), according to a series of experimental and theoretical investigations that will be discussed in detail in the following section. It is noteworthy that the yellow fluorescent band undergoes a pronounced quenching as the surface contamination increases (Fig. 3(a)), whereas the effect is considerably less pronounced on the blue band. This can be considered a ratiometric fluorescence response, a topic that has attracted considerable research

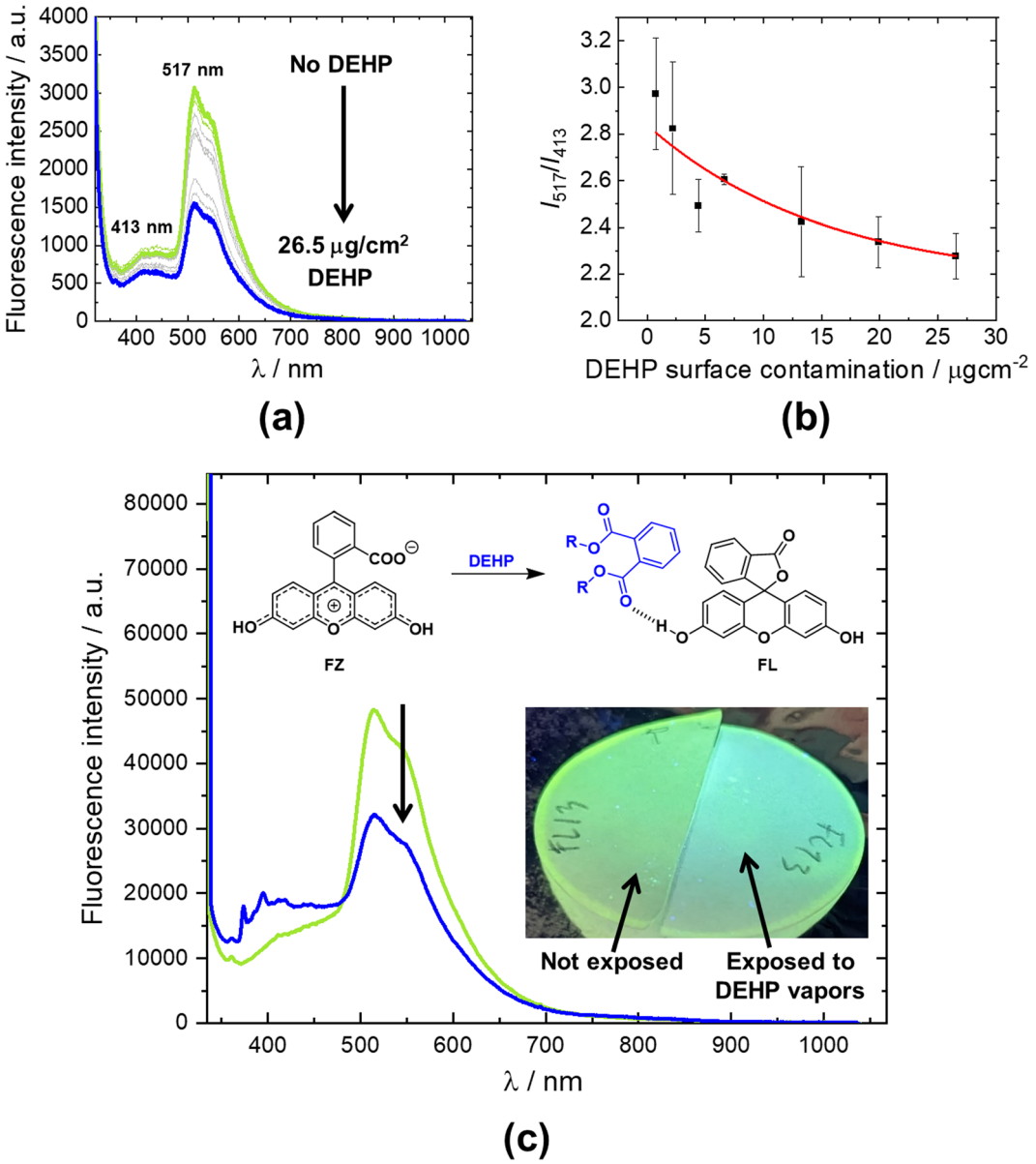

Fig. 3 Ratiometric fluorescent response towards **DEHP** and proposed detection mechanism for fluorescein test papers at λ_{exc} = 285 nm. (a) Representative example of the evolution of the fluorescence spectra with increasing **DEHP** surface contamination (b) Calibration curve built by plotting the ratio of fluorescent intensity at the two emission maxima (I_{517}/I_{413}) *versus* the **DEHP** surface contamination; the red line corresponds to an asymptotic decay fit of the data, $y = 2.156 + 0.682 \times 0.937^{x}$, with $R^2 = 0.77$ (c) Comparison of the fluorescence spectra and photograph of a test paper (under illumination with a λ = 254/365 nm handheld UV lamp), when not exposed and exposed to **DEHP** vapors (0.95 mbar, 13 days).

interest in recent years due to diverse analytical advantages,[18] including a more sensitive detection that frequently permits a naked-eye detection.[17] Furthermore, ratiometric sensors are self-calibrated, with the relatively unaltered fluorescent band serving as an internal reference for the concentration of the sensor. The measured property is consequently not monitored by the fluorescence intensity at either wavelength, but by their ratio. In the present case, the **DEHP** surface contamination is monitored by the ratio of the intensity of the yellow and blue bands (I_{517}/I_{413}).

It is important to highlight the significance of the above-mentioned self-calibration in the context of our research project. Potential variations in the fabrication of the test papers could produce inhomogeneities in the amount of fluorophore absorbed in different parts of the material. For classical fluorophores such as **F**, **FO**, **P** and **C**, such inhomogeneities can lead to changes in the fluorescence intensity not associated with the presence of the analyte, leading to erroneous **DEHP** surface contamination readings. The self-calibration in the case of **FL** ensures that variations in the fabrication of the test papers do not affect the **DEHP** surface contamination readings. Its ratiometric response is not dependent on the concentration of the fluorophore, but on the modulation of the I_{517}/I_{413} value, thus overcoming this problematic. Interestingly, the variation of

I_{517}/I_{413} with the **DEHP** surface contamination (from 0.74 to 26.55 μg cm^{-2}) leads to an apparent asymptotic decay (Fig. 3(b)). This implies that in the presence of **DEHP**, a portion of the zwitterionic species isomerizes to the lactoid tautomer (**FL**). Although the uncertainty in these measurements continue to be significant (0.9 to 10.0%), the isotherm for **FL** clearly demonstrates a higher sensitivity of this fluorophore towards **DEHP**, when compared to the other fluorophores studied in this work.

Once the calibration curve for the fluorescein test papers had been obtained, they were tested for the detection of phthalate vapors under the same conditions previously discussed for the other fluorophores. The results are illustrated in Fig. 3(c), depicting the identical ratiometric response observed when the materials were exposed to solutions of the contaminant, thereby providing compelling evidence of the efficacy of our materials for the visual detection of **DEHP** vapors. Moreover, thanks to the ratiometric response a color change is clearly observed by the naked eye, demonstrating the potential for real-time detection of the contaminant through visual observation, utilizing a handheld UV lamp to examine the material. In order to quantify the amount of **DEHP** vapors deposited on the test paper, the aforementioned asymptotic fit can be solved for the **DEHP** surface contamination, denoted as [**DEHP**], leading to eqn (2). The observed value obtained from the exposure to **DEHP** vapors is I_{517}/I_{413} = 1.69, which is below the minimum value required for direct use in this expression. Nevertheless, it can be stated with certainty that when exposed to **DEHP** vapors under these conditions, the surface contamination of the test paper is above 26.5 μg cm^{-2}, which represents the limit of the calibration curve.

$$[\mathbf{DEHP}]/\mu g\ cm^{-2} = \log_{0.937}\left(\frac{\frac{I_{517}}{I_{413}} - 2.156}{0.682}\right) \quad (2)$$

To summarize, this section presented the fluorescent response of the selected fluorophores to **DEHP**, which were identified as potential indicators of this contaminant by PET. With the exception of **C**, which exhibited an unstable fluorescent signal, all the fluorophores demonstrated the potential for application in the detection of the contaminant. This was evidenced by the recording of fluorescence changes using paper tests and a custom-built optical setup. The fluorescent response was found to align with the anticipated fluorescent quenching in the presence of **DEHP**, both in solution and as a vapor. The most notable optical response to **DEHP** was observed for **FL**, which exhibited a distinctive dual emission, enabling a ratiometric quantification and the potential for naked-eye detection, as significant advantages over the other fluorophores. Such response cannot possibly be attributed exclusively to PET and is associated with a **DEHP**-induced tautomerization of fluoresceine, a phenomenon that will be elaborated upon in the subsequent section.

It seems important to remark that while the determination of a precise limit of detection (LOD) value for the materials would be valuable, at present our developed methodology towards the detection of **DEHP** suffers from significant analytical limitations, as reflected in the important uncertainties in the calibration curves presented in Fig. 2 and 3(b). Due to this, the present investigation is limited to presenting a proof of concept for the new phthalate detection mechanisms, while refraining to report on LOD values. The analytical limitations of our methodology can be accounted to inhomogeneities in **DEHP** deposition and to experimental variations during data collection. Resolving these issues will require the use of alternative specialized equipment, such as that reported elsewhere for related materials targeting TNT detection.[11c]

Mechanistic insights and potential further applications for fluorescein

Fluorescein exists not only as the lactoid structure (**FL**) discussed in the previous sections, but also as two other tautomers (Scheme 1). These are the quinoid tautomer (**FQ**) where the fused tricyclic system adopts a xanthenone configuration, and the zwitterionic tautomer (**FZ**) with a negatively charged carboxylate and a positive charge delocalized within the fused tricyclic system. Considering the significant research interest and applications that fluorescein and its derivatives continue to attract, long after its first synthesis by von Baeyer in 1871,[19] it seems intriguing that its precise molecular structure, debated meticulously during the previous century,[20] continues to be scrutinized nowadays.[21] In this section we will briefly discuss some aspects of this complex topic, with the intention of clarifying and supporting our previous discussions on the **DEHP** sensing mechanism exhibited by fluorescein in the solid state, which was accounted to a tautomerization between the **FL** and **FZ** tautomers.

Our initial hypothesis regarding the dual blue/yellow (413/517 nm) emission observed during the investigations with this fluorophore using test papers was that the blue band originated from the FL tautomer while the yellow band from either **FQ** or **FZ**. The idea is supported by the fact that **FL** contains only small and poorly polarized π-systems isolated from each other due to interruption of electronic conjugation at the spirocyclic carbon. Consequently, its absorption and emission should be highly blue-shifted when compared to **FQ** and **FZ**, which feature an extended π-delocalization within the fused tricyclic submolecular fragment and a clear push–pull character in the case of **FQ**, where the hydroxyl and ketone groups act as electron donating and withdrawing groups, respectively.

In order to gain evidence for the above spectral assignments, an investigation was carried out aiming at isolating these tautomers in solution to compare their optical properties. The starting material was commercial fluorescein, which is sold as a red solid whose molecular structure is typically

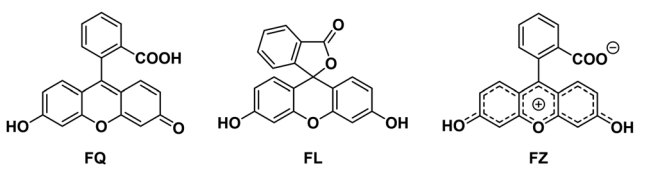

Scheme 1 The three different tautomers of neutral fluorescein: quinoid (**FQ**), lactoid (**FL**) and zwitterionic (**FZ**).

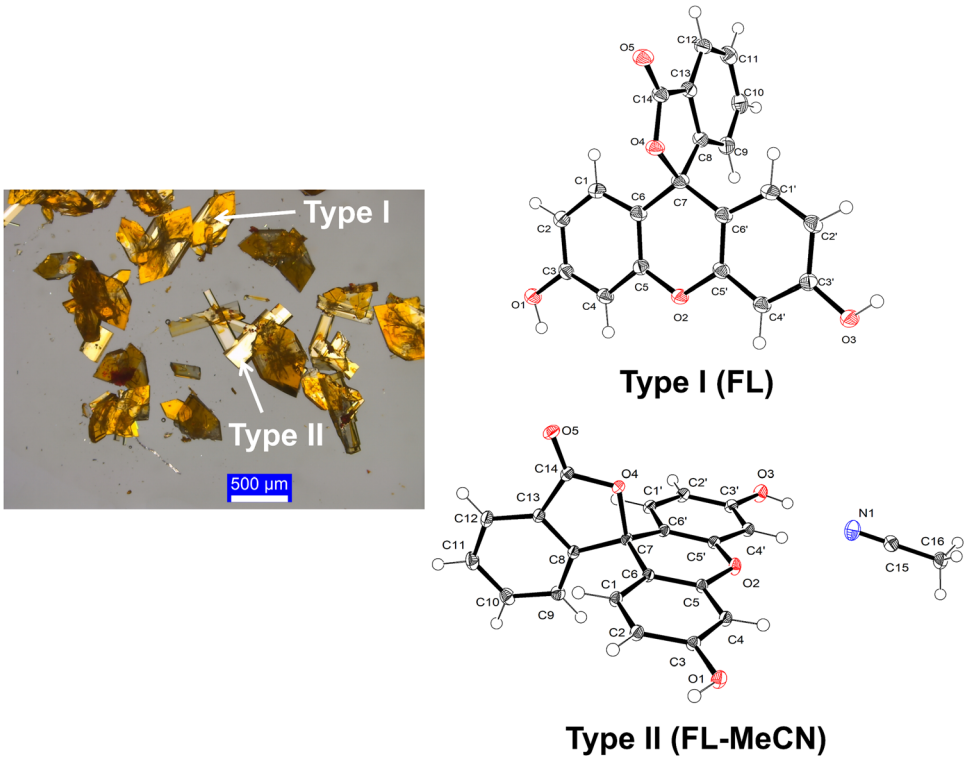

Fig. 4 Micrograph of crystals obtained from the slow evaporation of a saturated acetonitrile solution of the acetone solvate of fluorescein (**FL-Me$_2$CO**). Two types of colorless crystals, covered by a sticky yellowish solution, were obtained and diffracted. The crystal structures are shown in the right, corresponding to the solvent-free lactoid tautomer of fluorescein (**FL**) and its acetonitrile solvate (**FL-MeCN**). Thermal ellipsoids were drawn at 50% probability for every atom other than hydrogen. Selected bond lengths [Å] and angles [°] for **FL**: C3–O1 1.3616(15), C5–O2 1.3724(15), C7–O4 1.5093(14), C14–O5 1.2159(15), O4–C7–C6 108.70(10). For **FL-MeCN**: C3–O1 1.3507(11), C5–O2 1.3674(12), C7–O4 1.5110(12), C14–O5 1.2087(11), N1–O3 2.8420(18), N1–H3–O3 177.2(4), O4–C7–C6 107.02(7).

assigned to the **FQ** tautomer.[20b,21] Considering the transparency of acetonitrile in the near-UV region and for consistency with the rest of the study, the optical properties of fluorescein were first investigated in this solvent. Unfortunately, commercial fluorescein was found insoluble in acetonitrile, which was overcome by synthesizing an acetone solvate (**FL-Me$_2$CO**) that was gratifyingly found to be more soluble. The synthesis was carried out following a previously informed methodology[21] with minor modifications, and the procedure was further extrapolated to other unpublished solvates with dimethylformamide (**FL-DMF**) and dimethylsulfoxide (**FL-DMSO**) (details in ESI,† Section S6). In good agreement with previous research by the Jones group,[21,22] the syntheses involved a color change from red to yellow, due to a concomitant **FQ** → **FL** tautomerization. Besides the FT-IR/ATR and elemental analyses of these materials which confirmed their identity, we crystallized the **FL-Me$_2$CO** solvate by slow evaporation in acetonitrile, leading to two different types of crystals, which were studied by single-crystal X-ray diffraction (SXRD) and found to contain exclusively the **FL** tautomer (Fig. 4 and ESI,† Section S7). The first type of crystal corresponded to the solvent-free **FL** while the second was an acetonitrile solvate (**FL-MeCN**). It seems important to remark that to this appears to be the first report on the elusive crystal structure of **FL**, previously considered unlikely to exist due to thermodynamic instability in the absence of guest molecules.[21] While the bulk solids are indeed unstable when heated, as **FL** switches back to the **FQ** tautomer as solvents are removed, the phenomenon is different in the crystalline material, where the various strong supramolecular interactions (ESI,† Fig. S28 and S29) help stabilize the presence of solvent-free **FL** molecules.

With these two different types of fluorescein samples, *i.e.* commercial **FQ** and the various yellow **FL** solvates, a screening was performed to search for solvents where the optical properties of the different tautomers could be recorded. The identity of the fluorophore in various solvents was studied out using multinuclear $^{1}H/^{13}C$ NMR analyses. For clarity reasons, the details and further discussions of the NMR data are included in the ESI† (Section S8). The NMR studies on **FL-Me$_2$CO**, which was found soluble in CD_3CN, DMSO-d_6 and acetone-d_6, revealed the exclusive presence of the **FL** tautomer in solution, as evidenced by the signal for the spirocyclic carbon resonating around d = 83.08–83.92 ppm. On the other hand, **FQ** was soluble in DMSO-d_6 and acetone-d_6 and partially soluble in CD_3OD; NMR spectra in the former solvents were readily ascribed as well to the **FL** tautomer, implying a fast **FQ** → **FL** in these solvents. Contrastingly, the NMR spectra of **FQ** in CD_3OD was more complex, displaying an interesting temperature-dependent equilibrium between the **FL** and **FZ** tautomers. While at low temperature (T < 298 K) **FL** is again the only detectable species, at room and higher

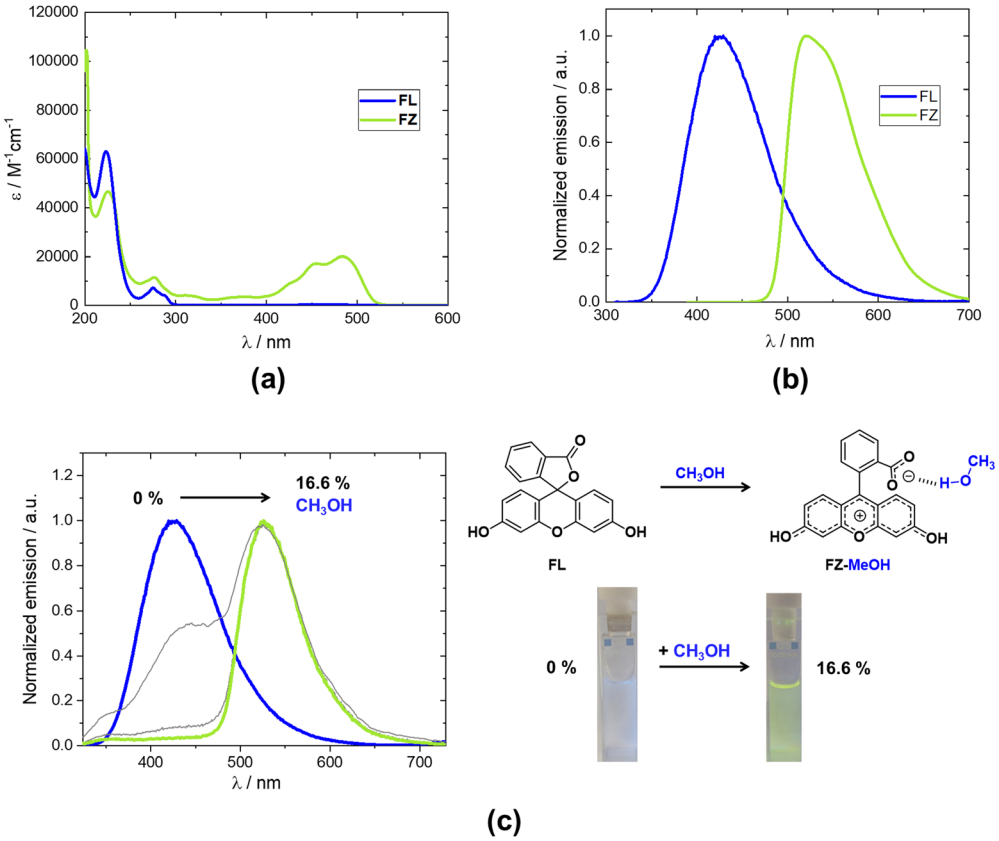

Fig. 5 Optical absorption (a) and emission (λ_{exc} = 285 nm) (b) spectra for fluorescein as its lactoid (**FL**) and zwitterionic (**FZ**) tautomers and (c) emission changes upon addition of up to 16.6% methanol to an acetonitrile solution of **FL**, inducing an **FL** → **FZ** tautomerization. As shown in the photographs, the change is observable by the naked under illumination using a λ = 254/365 nm handheld UV lamp. Spectra for **FZ** were recorded dissolving quinoid fluorescein (**FQ**) in methanol, while **FL** was recorded in acetonitrile from a freshly prepared analytical sample of the compound as an acetone solvate (**FL-Me$_2$CO**).

temperatures ($T \geq 298$ K) **FL** becomes undetectable, giving rise to a new C_2-symmetric species, which was assigned to the **FZ** tautomer, considering that the only alternative possibility would be **FQ**, but the C_2-symmetry is not expected for this tautomer and is indeed not observed for structurally-related fluorophores that are 'locked' in the same xanthenone configuration as **FQ**.[23]

These findings allowed a separate investigation of the optical properties of **FL** and **FZ** in solution, which to the best of our knowledge have never been published. Following our above discussions, spectra for **FL** were recorded from **FL-Me$_2$CO** in acetonitrile, while **FZ** was measured from methanol solutions of **FQ**. The results are presented in Fig. 5(a) and (b), where clear differences between both tautomers can be observed. In the case of **FL**, optical absorption and emission maxima are centered at λ_{abs} = 275 nm (ε = 7300 M^{-1} cm^{-1}) and λ_{em} = 425 nm, respectively, whereas **FZ** displayed strong bathochromic shifts, with absorption and emission maxima at λ_{abs} = 484 nm (ε = 20 000 M^{-1} cm^{-1}) and λ_{em} = 525 nm, respectively. These results constitute compelling evidence supporting the hypothesis that the **DEHP** sensing mechanism by fluorescein involves a tautomerization from a yellow-emissive (**FZ**) tautomer towards the blue-emissive **FL**. Indeed, the dual emission in the test papers (413 and 517 nm) lies extremely close to the values recorded for the individual tautomers in solution (425 and 525 nm), thus supporting the **FZ** → **FL** tautomerization as the ratiometric **DEHP** detection mechanism.

These fundamental findings also suggest additional interesting applications for this fluorophore. Indeed, the opposite tautomerization (**FL** → **FZ**) in solution can be envisioned to be applied for the fluorescent detection of alcohols, which is an area of current research interest.[24] An exploratory demonstration is shown in Fig. 5(c), where increasing amounts of methanol were added to an acetonitrile solution of **FL**, giving rise to the expected yellow emission from **FZ**, with the same effect being qualitatively observed when performing the test with ethanol. On the other hand, a **FL** → **FQ** tautomerization takes place in the solid state when the different **FL** solvates are heated, in good agreement with the first observations by the Jones group on the **FL-Me$_2$CO** solvate.[21] Interestingly, the color change that accompanies this transition could potentially be employed for the development of thermochromic materials, some of which benefit from irreversible thermochromic transitions[25] such as those provided by the solid state **FL** → **FQ** tautomerization. Furthermore, the thermogravimetric analyses for the different solvents, presented in ESI,† Fig. S27, show that the thermochromic transition is tuned depending on

the guest solvent, suggesting that the materials could be engineered to meet specific needs.

To finalize this section, we will present a brief discussion on the molecular mechanism behind these interesting equilibria. Although the experimental evidence discussed above explains the origins of the dual emission of fluorescein, which is modulated in the solid state by the presence of **DEHP**, these results were obtained in solution while detection of **DEHP** occurred in the solid state. Unfortunately, low fluorophore concentration renders instrumentally prohibitive to extend these analytical studies to the test papers to confirm that the same **FZ** → **FL** tautomerization induced by **DEHP** takes place also in the solid state. Nonetheless, a theoretical examination can provide the needed support for the molecular mechanism behind this transformation. In this sense, it is important to address first the implications surrounding the dissolution of commercial quinoid fluorescein (**FQ**) that leads to **FL** in most solvents or to a **FL** ↔ **FZ** equilibrium in methanol, while **FQ** is not found in solution in any of the organic solvents tested.

The first important observation is that switching from **FQ** to the other two tautomers implies a change in connectivity that cannot be explained without proton transfers. Fig. 6 depicts a potential mechanism accounting for these processes, along with a DFT-computed potential energy surface (PES) scan for the reaction. After getting solvated, **FQ** undergoes a solvent-mediated proton transfer through transition state **TS1** to reach the **FZ** tautomer, with methanol protonating the carbonyl group in **FQ**, while another proton is concertedly transferred from the carboxylic acid to methanol. It should be noted that the **FZ** tautomer was found unstable during the optimizations except if an explicit molecule of methanol was included. Consequently, this tautomer was computed as a methanol adduct (**FZ-MeOH**), which can finally tautomerize to **FL** without any proton transfer. The low computed activation energy to reach **TS1** (*ca.* 34.5 kJ mol^{-1}) agrees well with the fact that the whole process is experimentally observed at room temperature right after dissolving **FQ**. Additionally, the proposed mechanism is in line with the fact that the **FL** ↔ **FZ** equilibrium is also observed at room temperature, with **FL** being the dominant species at low temperature. Indeed, the PES scan shows **FL** as the most stable tautomer, separated to **FZ** by a low energy barrier (*ca.* 29.5 kJ mol^{-1}), which is accessible at room temperature and consequently in excellent agreement with the experimental evidence.

The most valuable information obtained from the above computational investigations is that the rapid equilibrium observed in the NMR experiments in CD_3OD can indeed be accounted to an interplay between the blue-emissive **FL** and the yellow-emissive **FZ**, and that room temperature is enough to shift the equilibrium towards **FZ** from the thermodynamically favored **FL** tautomer. Regarding the extrapolation of these results to the solid state, it seems plausible that the same equilibrium occurs within the test filter papers because these materials are mainly built from cellulose, which contains ubiquitous alkoxy groups that can play the same role of methanol in the stabilization of **FZ**. According to this, the **DEHP** sensing mechanism would involve a phthalate-induced

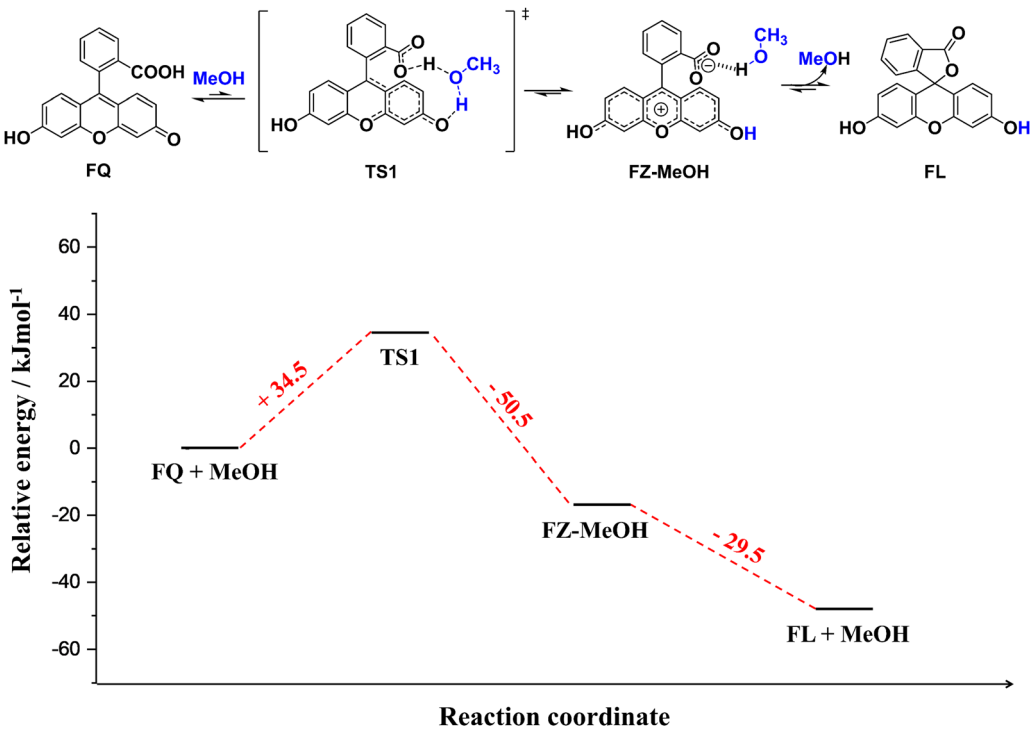

Fig. 6 Mechanism proposed for the tautomerization of commercial red quinoid fluorescein (**FQ**) towards the zwitterionic (**FZ**) and lactoid (**FL**) tautomers in methanol. A potential energy surface scan is shown in the bottom, as computed at the M06-2X/6-31+G(d,p)/PCM:Methanol level of theory. Energies are relative to that of **FQ** and a molecule of methanol computed at the same level of theory. Discontinuous red lines are indicative.

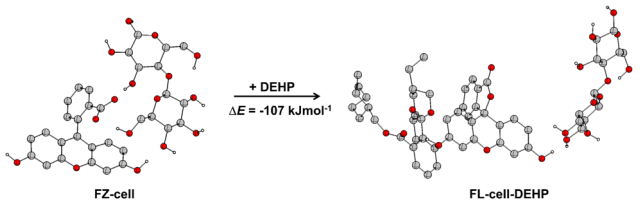

Fig. 7 Optimized molecular structure for adducts of zwitterionic fluorescein with a D-glucose dimer (**FZ-cell**) and of lactoid fluorescein with a D-glucose dimer and **DEHP** (**FL-cell-DEHP**). The potential energy change associated with this transformation, proposed to occur during the paper tests, is presented as computed at the M06-2X/6-31+G(d,p) level in vacuum. Hydrogens attached to carbon atoms are omitted for clarity.

FZ → **FL** tautomerization occurring within the test papers, as represented in Fig. 7, which shows DFT optimized models for the involved species. To reduce computational cost, a D-glucose dimer was used to represent cellulose, with the initial atomic coordinates extracted from the reported crystal structure.[26] These computations show that cellulose is indeed capable of stabilizing the zwitterionic tautomer, as demonstrated by the obtention of a stable structure for the adduct (**FZ-cell**), resembling the results described above for the **FZ-MeOH** adduct. The proposed transformation of **FZ-cell** towards a **DEHP** adduct where fluorescein tautomerizes to **FL** (**FL-cell-DEHP**) is indeed found to be significantly favored energetically by about 107 kJ mol^{-1}, thus providing theoretical support for the proposed **DEHP** sensing mechanism in the solid state.

Conclusion

This work was aimed at developing optical materials capable of detecting and quantifying **DEHP**, a plasticizer used in the manufacture of a myriad of daily-use goods and whose release from plastics has raised serious environmental and health concerns. Moreover, this contaminant also poses important problems for the proper functioning of optical devices in satellites and other spacecraft, on which it deposits as vapors and affects their performance. While several instrumental methods and sensors have been informed for the detection of **DEHP** and other phthalates in solution, optical sensors for vapors of these contaminants remain largely unexplored. We propose the use of fluorescence quenching through PET between **DEHP** and a given fluorophore as a sensing strategy. This process would compete with the emission of the fluorophore and thus result in fluorescence quenching in presence of the contaminant. Diverse computational and experimental investigations were carried out, leading to five potential fluorophores whose electronic properties were well-adapted for transferring an electron to **DEHP** upon photoexcitation. These fluorophores were subsequently tested against **DEHP** solutions and vapors using test papers, resulting in the anticipated quenching for three of them: 9*H*-fluorene, 9,9-dioctylfluorene and pyrene, with the latter showing the highest sensitivity among the three fluorophores. Although these results satisfactorily correlated with the pursued response of the materials, the sensitivity towards **DEHP** vapors was too low to allow practical applications.

The response of fluorescein, initially also envisioned for fluorescent detection by PET, was drastically different to that of the other fluorophores, offering an unparalleled sensitivity as well as an unanticipated naked-eye detection of the contaminant. These outstanding properties were associated with the dual emission of the materials, allowing a ratiometric detection with a higher visual contrast and sensitivity. Understanding the origins of this behavior required a thorough experimental and computational investigation that led to the conclusion that the dual emission stemmed from two different tautomers of fluorescein, the zwitterionic tautomer (**FZ**) and the lactoid tautomer (**FL**) with yellow and blue emission, respectively. Concurring experimental and computational evidence pointed towards a detection mechanism for the fluorescein-based materials involving an interesting solid-state **FZ** → **FL** tautomerization, accessible at room temperature and induced by **DEHP**. Besides our targeted applications for the detection of **DEHP**, the fundamental knowledge reported herein regarding the tautomerization of fluorescein could potentially prove useful for other applications, such as the detection of alcohols and the development of thermochromic materials.

Current work is being performed by our team for building a compact device implementing **FL** materials for the real-time monitoring of **DEHP** contamination in airspace missions. These compact devices will be comprised by a spectrometer, a light source, **FL** materials and a mechanical system to allow a quick and easy analysis in real time. The device will be tested in cleanrooms for monitoring molecular contamination before launch and possibly for in-flight experiments.

Regarding ratiometric fluorescent detection using materials built upon **FL**, the use of optical filters or other instrumentation allowing the isolation of each fluorescent band during data collection could be significantly beneficial for real-time monitoring of molecular contamination by phthalates.

Data availability

The data supporting this article have been included as part of the ESI.† Deposition Numbers 2407098 and 2407099 contain the supplementary crystallographic data for this paper. These data are provided by the joint Cambridge Crystallographic Data Centre and Fachinformationszentrum Karlsruhe Access Structures service.

Conflicts of interest

There are no conflicts to declare.

Acknowledgements

Authors acknowledge funding by the French space agency Centre National d'Etudes Spatiales (CNES). P. L.-V. gratefully acknowledges the CNES and Secretaría de Educación, Ciencia,

Tecnología e Innovación de la Ciudad de México (SECTEI) for their financial support to carry out this research. This work was granted access to the HPC resources of the CALMIP supercomputing centre under the allocations P21014. Authors gratefully acknowledge Céline Merlet and Julie Selegani from CIRIMAT for their support to access the HPC resources and for ATG analyses, respectively, as well as Sonia Mallet-Ladeira and Alix-Saquet from LCC-CNRS for their support with SXRD and CV analyses. We would finally like to express our gratitude to Yannick Coppel and Christian Bijani from LCC-CNRS for their support and helpful discussions on NMR analyses.

Notes and references

1 (*a*) H. Tuan Tran, C. Lin, X.-T. Bui, M. Ky Nguyen, N. Dan Thanh Cao, H. Mukhtar, H. Giang Hoang, S. Varjani, H. Hao Ngo and L. D. Nghiem, Phthalates in the environment: characteristics, fate and transport, and advanced wastewater treatment technologies, *Bioresour. Technol.*, 2022, **344**, 126249; (*b*) A. Pagoni, O. S. Arvaniti and O.-I. Kalantzi, Exposure to phthalates from personal care products: Urinary levels and predictors of exposure, *Environ. Res.*, 2022, **212**, 113194.

2 (*a*) A. Wilson, *Plasticizers: Principles and Practice*, The Institute of Materials, London, Rakow, NA, 1995; (*b*) G. Wypych, *Handbook of plasticizers*, 2004, pp. 7–71.

3 (*a*) W. M. Kluwe, E. E. McConnell, J. E. Huff, J. K. Haseman, J. F. Douglas and W. V. Hartwell, Carcinogenicity testing of phthalate esters and related compounds by the National Toxicology Program and the National Cancer Institute, *Environ. Health Perspect.*, 1982, **45**, 129–133; (*b*) P. M. D. Foster, E. Mylchreest, K. W. Gaido and M. Sar, Effects of phthalate esters on the developing reproductive tract of male rats, *Hum. Reprod. Update*, 2001, **7**, 231–235; (*c*) L. G. Parks, J. S. Ostby, C. R. Lambright, B. D. Abbott, G. R. Klinefelter, N. J. Barlow and L. E. Gray, Jr., The Plasticizer Diethylhexyl Phthalate Induces Malformations by Decreasing Fetal Testosterone Synthesis during Sexual Differentiation in the Male Rat, *Toxicol. Sci.*, 2000, **58**, 339–349.

4 E. C. Regulation, OJ L 2008, 353.

5 Q. Luo, Z.-h Liu, H. Yin, Z. Dang, P.-x Wu, N.-w Zhu, Z. Lin and Y. Liu, Migration and potential risk of trace phthalates in bottled water: A global situation, *Water Res.*, 2018, **147**, 362–372.

6 P. Labra-Vázquez, M. Gressier, G. Rioland and M.-J. Menu, A review on solution- and vapor-responsive sensors for the detection of phthalates, *Anal. Chim. Acta*, 2023, **1282**, 341828.

7 D. Ferguson, P. Crabtree, S. White and B. Vayner, Anomalous Global Positioning System Power Degradation from Arc-Induced Contamination, *J. Spacecr. Rockets*, 2016, **53**, 464–470.

8 (*a*) V. Haemmerle and J. Gerhard, Cassini Camera Contamination Anomaly: Experiences and Lessions Learned, in SpaceOps 2006 Conference; (*b*) J. MacKenty, G. Schneider, S. Baggett, D. Mitchell, C. Ritchie and W. Sparks, *On-orbit management of contaminants within the Hubble Space Telescope widefield planetary camera and their effect on instrument performance*, SPIE, 1993, vol. 1945.

9 C. Qiu, Y. Gong, Y. Guo, C. Zhang, P. Wang, J. Zhao and Y. Che, Sensitive Fluorescence Detection of Phthalates by Suppressing the Intramolecular Motion of Nitrophenyl Groups in Porous Crystalline Ribbons, *Anal. Chem.*, 2019, **91**, 13355–13359.

10 (*a*) F. Sebák, L. B. Horváth, D. Kovács, J. Szolomájer, G. K. Tóth, Á. Babiczky, S. Bősze and A. Bodor, Novel Lysine-Rich Delivery Peptides of Plant Origin ERD and Human S100: The Effect of Carboxyfluorescein Conjugation, Influence of Aromatic and Proline Residues, Cellular Internalization, and Penetration Ability, *ACS Omega*, 2021, **6**, 34470–34484; (*b*) C. Munkholm, D. R. Parkinson and D. R. Walt, Intramolecular fluorescence self-quenching of fluoresceinamine, *J. Am. Chem. Soc.*, 1990, **112**, 2608–2612; (*c*) L. D. Lavis and R. T. Raines, Bright Building Blocks for Chemical Biology, *ACS Chem. Biol.*, 2014, **9**, 855–866; (*d*) M. D. Hammers, M. J. Taormina, M. M. Cerda, L. A. Montoya, D. T. Seidenkranz, R. Parthasarathy and M. D. Pluth, A Bright Fluorescent Probe for H_2S Enables Analyte-Responsive, 3D Imaging in Live Zebrafish Using Light Sheet Fluorescence Microscopy, *J. Am. Chem. Soc.*, 2015, **137**, 10216–10223; (*e*) T. Aslam, A. Miele, S. V. Chankeshwara, A. Megia-Fernandez, C. Michels, A. R. Akram, N. McDonald, N. Hirani, C. Haslett, M. Bradley and K. Dhaliwal, Optical molecular imaging of lysyl oxidase activity – detection of active fibrogenesis in human lung tissue, *Chem. Sci.*, 2015, **6**, 4946–4953; (*f*) J. E. T. Corrie and D. R. Trentham, Synthesis of photoactivatable fluorescein derivatives bearing side chains with varying properties, *J. Chem. Soc., Perkin Trans. 1*, 1995, 1993–2000; (*g*) M. Rajasekar, Recent development in fluorescein derivatives, *J. Mol. Struct.*, 2021, **1224**, 129085; (*h*) J. B. Grimm, A. J. Sung, W. R. Legant, P. Hulamm, S. M. Matlosz, E. Betzig and L. D. Lavis, Carbofluoresceins and Carborhodamines as Scaffolds for High-Contrast Fluorogenic Probes, *ACS Chem. Biol.*, 2013, **8**, 1303–1310.

11 (*a*) H. Niu, J. Liu, H. M. O'Connor, T. Gunnlaugsson, T. D. James and H. Zhang, Photoinduced electron transfer (PeT) based fluorescent probes for cellular imaging and disease therapy, *Chem. Soc. Rev.*, 2023, **52**, 2322–2357; (*b*) G. L. Gaines, III, M. P. O'Neil, W. A. Svec, M. P. Niemczyk and M. R. Wasielewski, Photoinduced electron transfer in the solid state: rate vs. free energy dependence in fixed-distance porphyrin-acceptor molecules, *J. Am. Chem. Soc.*, 1991, **113**, 719–721; (*c*) L. Mosca, R. S. Khnayzer, M. S. Lazorski, E. O. Danilov, F. N. Castellano and P. Anzenbacher Jr., Sensing of 2,4,6-Trinitrotoluene (TNT) and 2,4-Dinitrotoluene (2,4-DNT) in the Solid State with Photoluminescent RuII and IrIII Complexes, *Chem. – Eur. J.*, 2015, **21**, 4056–4064.

12 (*a*) E. M. Espinoza, J. A. Clark, J. Soliman, J. B. Derr, M. Morales and V. I. Vullev, Practical Aspects of Cyclic Voltammetry: How to Estimate Reduction Potentials When Irreversibility Prevails, *J. Electrochem. Soc.*, 2019, **166**,

H3175–H3187; (*b*) D. M. de Leeuw, M. M. J. Simenon, A. R. Brown and R. E. F. Einerhand, Stability of N-Type Doped Conducting Polymers and Consequences for Polymeric Microelectronic Devices, *Synth. Met.*, 1997, **87**, 53–59.

13 (*a*) X. Zheng, A. J. Cohen, P. Mori-Sánchez, X. Hu and W. Yang, Improving Band Gap Prediction in Density Functional Theory from Molecules to Solids, *Phys. Rev. Lett.*, 2011, **107**, 026403; (*b*) P. Borlido, T. Aull, A. W. Huran, F. Tran, M. A. L. Marques and S. Botti, Large-Scale Benchmark of Exchange–Correlation Functionals for the Determination of Electronic Band Gaps of Solids, *J. Chem. Theory Comput.*, 2019, **15**, 5069–5079; (*c*) K. Sohlberg and M. E. Foster, What's the gap? A possible strategy for advancing theory, and an appeal for experimental structure data to drive that advance, *RSC Adv.*, 2020, **10**, 36887–36896.

14 (*a*) M. E. El-Khouly, O. Ito, P. M. Smith and F. D'Souza, Intermolecular and supramolecular photoinduced electron transfer processes of fullerene–porphyrin/phthalocyanine systems, *J. Photochem. Photobiol., C*, 2004, **5**, 79–104; (*b*) J. Fajer, K. M. Barkigia, D. Melamed, R. M. Sweet, H. Kurreck, J. von Gersdorff, M. Plato, H. C. Rohland, G. Elger and K. Möbius, Molecular Structures of Porphyrin−Quinone Models for Electron Transfer, *J. Phys. Chem.*, 1996, **100**, 14236–14239.

15 (*a*) D. Rehm and A. Weller, Kinetics of Fluorescence Quenching by Electron and H-Atom Transfer, *Isr. J. Chem.*, 1970, **8**, 259–271; (*b*) D. Kim and T. S. Teets, Strategies for accessing photosensitizers with extreme redox potentials, *Chem. Phys. Rev.*, 2022, **3**, 021302.

16 (*a*) J. Verhoeven, Through-bond charge transfer interaction and photoinduced charge separation, *Pure Appl. Chem.*, 1986, **58**, 1285–1290; (*b*) N. J. Turro, V. Ramamurthy and J. C. Scaiano, *Principles of molecular photochemistry: an introduction*, University science books, 2009.

17 K. Zhang, H. Zhou, Q. Mei, S. Wang, G. Guan, R. Liu, J. Zhang and Z. Zhang, Instant Visual Detection of Trinitrotoluene Particulates on Various Surfaces by Ratiometric Fluorescence of Dual-Emission Quantum Dots Hybrid, *J. Am. Chem. Soc.*, 2011, **133**, 8424–8427.

18 (*a*) J. Zhang, H. Chen, K. Xu, D. Deng, Q. Zhang and L. Luo, Current Progress of Ratiometric Fluorescence Sensors Based on Carbon Dots in Foodborne Contaminant Detection, *Biosensors*, 2023, **13**, 233; (*b*) J. Chi, Y. Song and L. Feng, A ratiometric fluorescent paper sensor based on dye-embedded MOF for high-sensitive detection of arginine, *Biosens. Bioelectron.*, 2023, **241**, 115666; (*c*) H.-Q. Yin, J.-C. Yang and X.-B. Yin, Ratiometric Fluorescence Sensing and Real-Time Detection of Water in Organic Solvents with One-Pot Synthesis of Ru@MIL-101(Al)–NH_2, *Anal. Chem.*, 2017, **89**, 13434–13440.

19 A. Baeyer, Ueber eine neue Klasse von Farbstoffen, *Ber. Dtsch. Chem. Ges.*, 1871, **4**, 555–558.

20 (*a*) W. R. Orndorff and A. Hemmer, Fluorescein and some of its derivatives, *J. Am. Chem. Soc.*, 1927, **49**, 1272–1280; (*b*) R. Markuszewski and H. Diehl, The infrared spectra and structures of the three solid forms of fluorescein and related compounds, *Talanta*, 1980, **27**, 937–946.

21 M. Arhangelskis, M. D. Eddleston, D. G. Reid, G. M. Day, D.-K. Bučar, A. J. Morris and W. Jones, Rationalization of the Color Properties of Fluorescein in the Solid State: A Combined Computational and Experimental Study, *Chem. – Eur. J.*, 2016, **22**, 10065–10073.

22 D.-K. Bučar, S. Filip, M. Arhangelskis, G. O. Lloyd and W. Jones, Advantages of mechanochemical cocrystallisation in the solid-state chemistry of pigments: colour-tuned fluorescein cocrystals, *CrystEngComm*, 2013, **15**, 6289–6291.

23 V. Trovato, G. Rosace, C. Colleoni and M. R. Plutino, Synthesis and characterization of halochromic hybrid sol–gel for the development of a pH sensor fabric, *IOP Conf. Ser.: Mater. Sci. Eng.*, 2017, **254**, 072027.

24 (*a*) P. D. Thungon, H. Wang, S. I. Vagin, C. V. Dyck, P. Goswami, B. Rieger and A. Meldrum, A Fluorescent Alcohol Biosensor Using a Simple microPAD Based Detection Scheme, *Front. Sens.*, 2022, **3**, 840130; (*b*) Y. Chen, W. Chen, Y. Tian, P. Zhu, S. Liu, L. Du and C. Wu, DNA and RhoB-functionalized metal–organic frameworks for the sensitive fluorescent detection of liquid alcohols, *Microchem. J.*, 2021, **170**, 106688; (*c*) M. Akamatsu, T. Mori, K. Okamoto, H. Komatsu, K. Kumagai, S. Shiratori, M. Yamamura, T. Nabeshima, H. Sakai, M. Abe, J. P. Hill and K. Ariga, Detection of Ethanol in Alcoholic Beverages or Vapor Phase Using Fluorescent Molecules Embedded in a Nanofibrous Polymer, *ACS Appl. Mater. Interfaces*, 2015, **7**, 6189–6194.

25 (*a*) D. K. Nguyen, Q.-V. Bach, J.-H. Lee and I.-T. Kim, Synthesis and Irreversible Thermochromic Sensor Applications of Manganese Violet, *Materials*, 2018, **11**, 1693; (*b*) I. Kalinke and U. Kulozik, Irreversible thermochromic ink in the identification of over- and under-processed product segments in microwave-assisted freeze drying, *J. Food Eng.*, 2023, **349**, 111470; (*c*) A. Hakami, S. S. Srinivasan, P. K. Biswas, A. Krishnegowda, S. L. Wallen and E. K. Stefanakos, Review on thermochromic materials: development, characterization, and applications, *J. Coat. Technol. Res.*, 2022, **19**, 377–402.

26 Y. Nishiyama, P. Langan and H. Chanzy, Crystal Structure and Hydrogen-Bonding System in Cellulose Iβ from Synchrotron X-ray and Neutron Fiber Diffraction, *J. Am. Chem. Soc.*, 2002, **124**, 9074–9082.

